energy&fuels

Article

pubs.acs.org/EF

Effects of Secondary Air on Flow, Combustion, and NO_x Emission from a Novel Pulverized Coal Burner for Industrial Boilers

Gong-Gang Sun,[†,‡] De-Fu Che,*[,†] and Zuo-He Chi[‡]

[†]School of Energy and Power Engineering, Xi'an Jiaotong University, Xi'an 710049, China

[‡]College of Metrological and Measurement Engineering, China Jiliang University, Hangzhou 310018, China

ABSTRACT: This paper deals with an experimental investigation on the performance of a novel pulverized coal burner, featuring the introduction of an outer secondary air without swirling, as applied to an industrial boiler. Both cold air and combustion tests were conducted to investigate the effects of the secondary air on flow, combustion, and NO_x emission from this novel burner. The measured flow fields, temperature distributions, and gas concentrations were presented. It was shown that, due to the presence of the outer secondary air, slagging in the adiabatic combustion chamber could be avoided and a NO_x emission level of 600 mg/Nm^3 was realized. In addition, the operating efficiency of the boiler was found to be greater than 89.50%, which was higher than that of the conventional industrial boilers.

1. INTRODUCTION

In China, there are currently about 600 000 industrial boilers in use, and most of them are coal-fired boilers such as traveling grate-firing boilers. More than 400 million tons of coal is consumed annually by industrial boilers with an average efficiency of 60−70%. Industrial coal-fired boilers have been identified as one of the main contributors to air pollution.[1] To reduce the pollutant emissions associated with coal-based energy conversion, oil- and natural gas-fired boilers have been promoted recently. Scaling up the utilization of such coal-free boilers, however, is restricted because China has much poorer reserve in oil and natural gas than coal.

As an alternative solution, a portion of the existing coal- and oil-fired industrial boilers in China have been retrofitted so as to use coal−water slurry (CWS) as the fuel since the late 1990s.[2] By means of replacing the original burners with CWS burners, adding pulping systems, as well as retrofitting the furnaces and slag removal systems, the operating efficiency of the retrofitted boilers has become greater than 80%.[3] Despite higher efficiency and low pollutant emissions associated with the retrofitted boilers, penalties have been realized, including slagging near the exit of CWS burners, and especially greater oil consumption for furnace heating during start-up of the boilers. In addition, heating, evaporation, and vaporization of water in CWS that absorb the heat from the furnaces slightly lowers the operating efficiency of the boilers.

A higher efficiency can be achieved if pulverized coal (PC), instead of CWS, is utilized as the fuel for industrial boilers. The earliest attempt in China may be dated back to the late 1980s when the retrofitting work on a 4 t/h fixed grate-firing boiler was reported by Feng.[4] A swirl burner was installed on the side wall of the furnace to introduce the primary air (PA) through a volute, thus leading to swirling of the PA that mixes strongly with the single-stage swirling secondary air (SA) in the adiabatic combustion chamber (ACC) where the coal particles are ignited and combusted before entering the furnace. By doing so, the operating efficiency of the retrofitted boiler attained 73−75% and the unburned carbon in fly ash was less than 5%. Pronounced slagging in the ACC, however, was observed due to the high volumetric heat release rate associated with this swirl burner. Later on, Pang et al.[5] proposed a design of PC burner in which the PA is also introduced swirly, whereas the SA is separated into three portions that are introduced tangentially into the ACC and mix with the PA individually. The original 4 t/h oil- and natural gas-fired boiler was successfully retrofitted to use PC by replacing the original burner with this newly designed one. The operating efficiency and unburned carbon in fly ash of the retrofitted boiler were found to be 75% and 7%, respectively. Slagging was also observed in the ACC in this work. To mitigate slagging, Ji[6] proposed recently another design of PC burners for industrial boilers, in which the wall of the ACC was water-cooled in an effort to reduce the local volumetric heat release rate in the vicinity of the wall. The PA of the burner was introduced directly into the ACC and then reflected backward by a reflective cap to allow mixing with the single-stage swirling SA. The retrofitted burner was used in a 4 t/h steam boiler firing PC. Although slagging was mitigated in the ACC and an operating efficiency of 86% was attained, a penalty was found that the unburned carbon in fly ash was as high as 25% due to the reduced volumetric heat release rate in the ACC.

In light of the previous attempts, it is obvious that the design of an efficient PC burner is the key to achieving a compromise between low slagging tendency and high combustion efficiency. The inclusion of outer SA has been attempted intensively in the literature,[7−14] and this technique has shown to be a promising solution. Swirling outer SA, however, was used in all the above-mentioned studies. In this paper, a novel design of PC burners for industrial boilers will be proposed that features the utilization of outer SA without swirling. This design will be expected to enable complete and stable combustion of PC in the ACC without slagging. Cold air tests will be carried out to

Received: June 20, 2012
Revised: October 3, 2012
Published: October 3, 2012

dx.doi.org/10.1021/ef301043x | *Energy Fuels* 2012, 26, 6640−6650

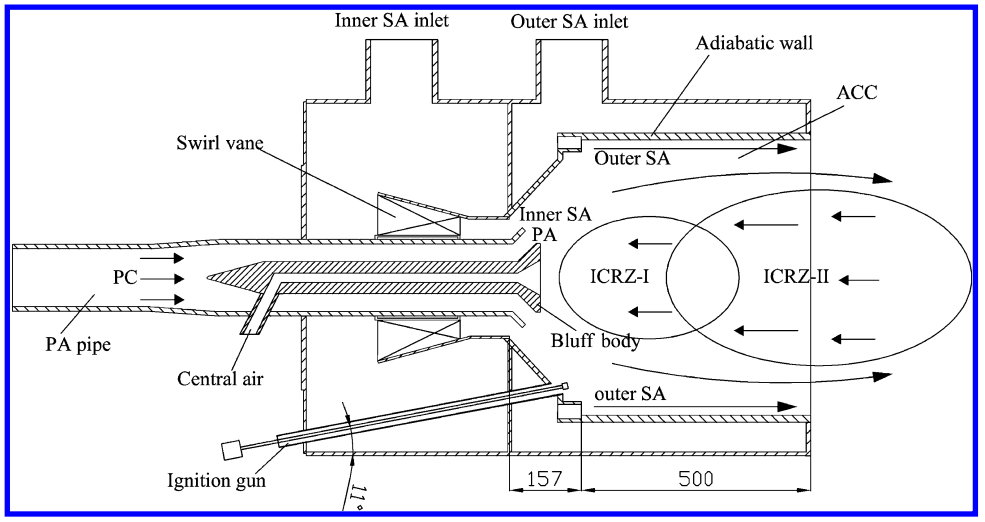

Figure 1. Design and geometric dimensions of the novel PC burner (unit: mm).

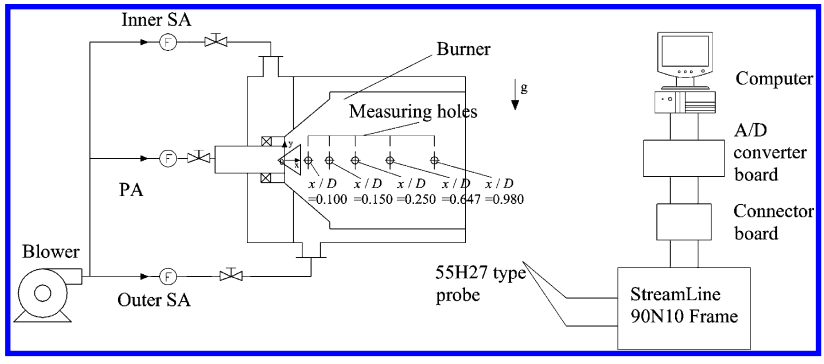

Figure 2. Schematic diagram of the experimental setup for cold air tests.

analyze the influence of SA on aerodynamic behaviors of the burner with this novel design. The performance of the boiler will be assessed experimentally, and the effects of SA on coal combustion, gas temperature distributions, and NO_x emission in both the burner and furnace will be studied as well.

2. DESIGN OF THE NOVEL PC BURNER

The novel patented design of a PC burner[15] for industrial boilers is shown in Figure 1 with dimensions. The PC stream is introduced through the annular channel between the PA and central air pipes into the ACC. PA passing through the bluff body is injected into the ACC, thus creating an internal center recirculation zone (ICRZ)-I, as shown in Figure 1. This ICRZ-I leads to the opportunity for the high-temperature flue gases (HTFG) to flow backward from the ACC, forming a hot-gas reverse and an additional heat source near the exit of the PA nozzle. In the ACC, the swirling inner SA creates the ICRZ-II and leads to back-flowing HTFG in the furnace. As a result, HTFG are introduced continuously into the exit of the PA nozzle to heat up the PA. The combination of the overlaid two ICRZs assures rapid ignition of coal particles and desirable flame stability.

As shown in Figure 1, the novelty of this design lies in the inclusion of an outer SA that sweeps along the wall of the ACC, in an effort to avoid slagging, which also leads to reduction of NO_x emission because of air-staged combustion.

3. METHODOLOGY

3.1. Cold Air Tests. The cold air tests were carried out on a full-scale PC burner with the novel design that was later utilized in combustion tests. The test facility for cold air experiments was constructed, as illustrated schematically in Figure 2. It is noted that only the burner was included in this test facility and the burner exit was directly exposed to ambient air. A local Cartesian coordinate system was adopted in such a way that the origin is placed at the center of the inner SA exit plane, x-axis is along the jet flow direction, and y-axis is along the radius opposite to gravity. Measuring holes were reserved on the side wall of the burner along the x-axis at an increasing spacing, as sketched in Figure 2.

As shown in Figure 2, the air flow rates of the PA, inner SA, and outer SA were controlled using butterfly valves arranged on the individual air pipes. The flow rates were measured using pitot tubes that were calibrated with an uncertainty of 4.5%. The design parameters of the PC burner with 10 bent-shaft vanes in the inner SA duct are given in Table 1. Effects of swirling intensity of the inner SA on the flow fields were examined by altering the swirl vane angles from 30 to 60°, as demonstrated in Figure 3.

The swirling intensity Ω of the inner SA may be calculated by

$$\Omega = M/(KL) \quad (1)$$

where M, K, and L are the rotary momentum moment (kg m^2/s^2), axial momentum (kg m/s^2), and characteristic length (m), respectively, which are defined as

dx.doi.org/10.1021/ef301043x | Energy Fuels 2012, 26, 6640−6650

Table 1. Design Parameters of the Novel PC Burner

items	novel PC burner
exit area of the PA (m^2)	0.0137
exit area of the inner SA (m^2)	0.0214
exit area of the outer SA (m^2)	0.0094
temp. of the PA (°C)	20.0
temp. of the inner SA (°C)	20.0
temp. of the outer SA (°C)	20.0
mass flow rate of the PA (kg s^{-1})	0.36
mass flow rate of the inner SA (kg s^{-1})	0.65
mass flow rate of the outer SA (kg s^{-1})	0.29
diam. of the ACC (mm)	600
diam. of the PA pipe (mm)	126

$$M = \rho q \omega_t r \quad (2)$$

$$K = \rho q \omega_a \quad (3)$$

and

$$L = \pi r/4 \quad (4)$$

with ρ being the density (kg/m^3), q the volumetric flow rate (m^3/s), ω_t the tangential velocity (m/s), ω_a the axial velocity (m/s), and r the rotation radius of the stream (m).

Given the parameters, the swirling intensities of the inner SA for swirl vane angle at 30, 45, and 60° were determined to be 0.74, 1.27, and 2.21, respectively. In the experiments, three-dimensional isothermal flow fields in the ACC were measured by employing a Dantec Streamline 90N10 frame constant temperature anemometer with a cross-wire probe (55H27 type). The uncertainty of velocity measurements was calibrated to be less than 5%. In an effort to determine the boundary of the ICRZ, a ribbon was fixed on a moving coordinate frame that was installed in the ACC.

3.2. Combustion Tests. *3.2.1. Experimental Setup.* In addition to the cold air experiments, a series of combustion tests were conducted with a full-scale SZS-1.25/4-M industrial boiler, as shown in Figure 4. The design parameters of the boiler are listed in Table 2. The furnace of the boiler that was 1.4 × 2 × 5 m^3 in size, as demonstrated in Figure 5, was covered by a water-cooled jacket with an outer layer of a refractory material. The burner, which was installed on the front wall of the furnace, was made of stainless steel and an insulation material for the ACC.

As shown in Figure 5, the Cartesian coordinate system defined in Figure 2 was retained. A monitoring hole was located on the side wall of the burner, whereas a total number of five monitoring holes were reserved for the furnace, four of which were located on the side wall with the remaining one on the rear wall.

3.2.2. Fuel Properties. The ultimate and proximate analyses and the lower heating value of the coal used in this work are given in Table 3. The size of the coal particles ranged from 1 to 120 μm with a mean value of 40 μm.

3.2.3. Experimental Procedure. The coal particles were milled and stored in a hopper under dry condition before use. A blower supplied the combustion air into the pipes of PA, inner SA, and outer SA separately. As illustrated in Figure 4, PC was fed through a screw feeder, mixed with PA in the venturi mixer, and then injected into the burner. The boiler start-up process was initiated by ignition of a liquefied petroleum gas (LPG) torch with an ignition gun inserted in the ACC at an inclination angle of 11°. The LPG torch supplied the HTFG for the ICRZs to ignite the PC within an extremely short time period after PC is fed. During the combustion tests, the boiler operated stably with a full load.

Gas temperatures were measured using a type-S thermocouple (TC) mounted inside a water-cooled stainless-steel probe for gas sampling. The temperature readings may be overestimated due to radiative heating by the high-temperature flame on the bare bead of the TC. The presence of radiative heat loss of the TC bead to the water-cooled wall, however, might lead to underestimated temperature readings. The uncertainty of the measured local gas temperature was within ±50 °C.

After passing through a filtration device, the gas samples were analyzed with an MRU gas analyzer (MGA 5), determining concentrations of O_2, CO, NO, and NO_2. The accuracy of the gas analyzer was 0.2% for O_2 and 5% for CO, NO, and NO_2. The sensors involved were calibrated before measurement. During the combustion tests, the fly ash was sampled at the sampling hole located between the economizer and the dust

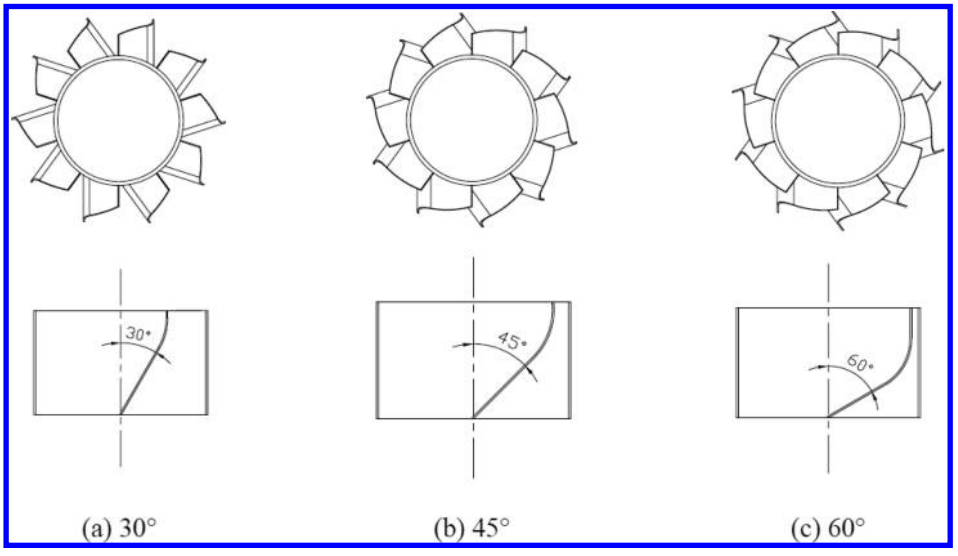

Figure 3. Sketch of the swirl vane at different angles.

dx.doi.org/10.1021/ef301043x | *Energy Fuels* 2012, 26, 6640−6650

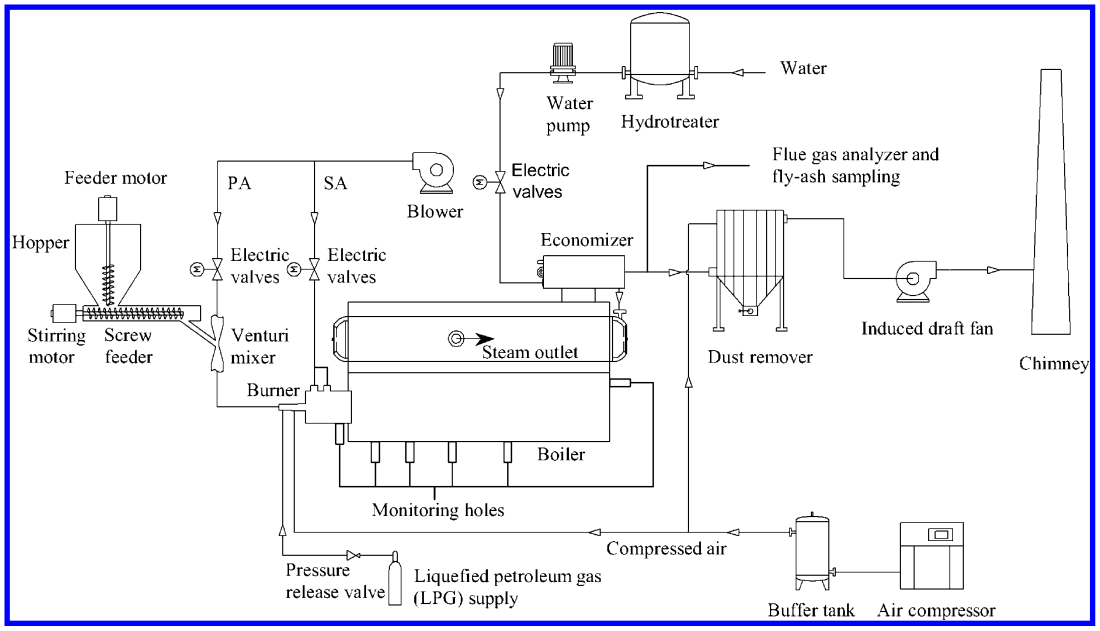

Figure 4. Schematic diagram of the experimental setup for combustion tests.

Table 2. Design Parameters of the SZS-1.25/4-M Type Industrial Boiler

items	design param.
flow rate of the steam (t h^{-1})	4
pressure of the steam (MPa)	1.25
water feeding temp. (°C)	20.0
coal feeding rate (kg h^{-1})	472
vol. of furnace (m^3)	16.0
area of radiation heated surface (m^2)	27.0
area of convection heated surface (m^2)	100.0

Table 3. Characteristics of the Coal Used in the Experiments

ultimate analysis (as received, wt%)				
carbon	hydrogen	sulfur	nitrogen	oxygen
68.27	5.19	0.43	0.88	10.51
proximate: analysis (as received, wt%)				
volatiles	ash	moisture	fixed carbon	lower heating value (kJ/kg)
34.11	7.11	7.61	51.17	27,300

remover, as shown in Figure 4. The unburned carbon in fly ash was determined using the gravimetric technique.

4. RESULTS AND DISCUSSION

In the present study, the characteristics of flow, combustion, and NO_x emission resulting from the novel PC burner were studied experimentally at various inner SA swirling intensities. The effect of the outer SA on slagging was also examined.

4.1. Flow Fields. The profiles of the measured axial, tangential, and radial velocity components from the cold air tests over cross-sectional slices at various axial locations are presented in Figures 6, 7, and 8, respectively. These locations are labeled in Figure 2. As shown in Figure 6, two peaks along the radial direction exist on the curves of the axial velocity component in the first two slices (x/D = 0.100 and 0.150 where D is the diameter of the ACC) for all the three swirling intensities. The outer peak near the wall of the burner is due to the inner SA stream, whereas the inner one near the bluff body is generated by the PA flow. Mixing of the PA and SA develops quickly due to the high velocity gradient between them, thus leading to a local area with a high mass-transfer rate. The PA has completely merged into the inner SA for $x/D \geq 0.250$,

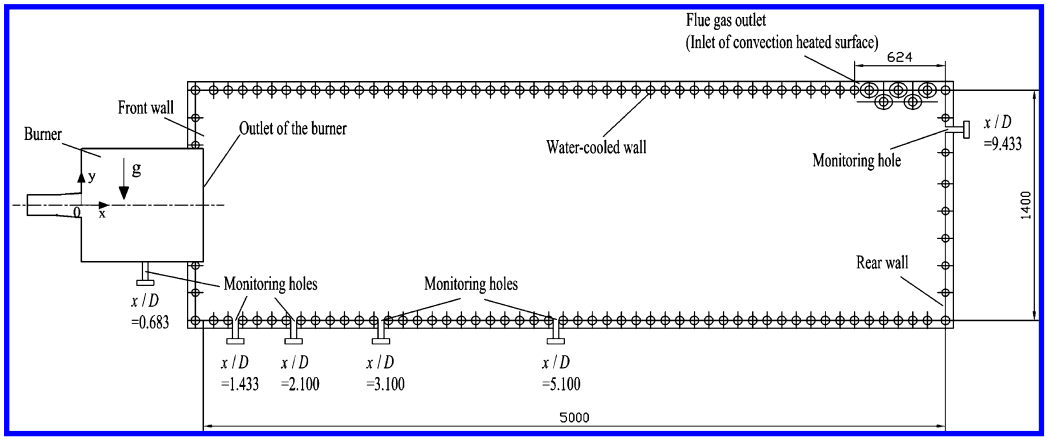

Figure 5. Design and geometric dimensions of the furnace (unit: mm).

dx.doi.org/10.1021/ef301043x | Energy Fuels 2012, 26, 6640−6650

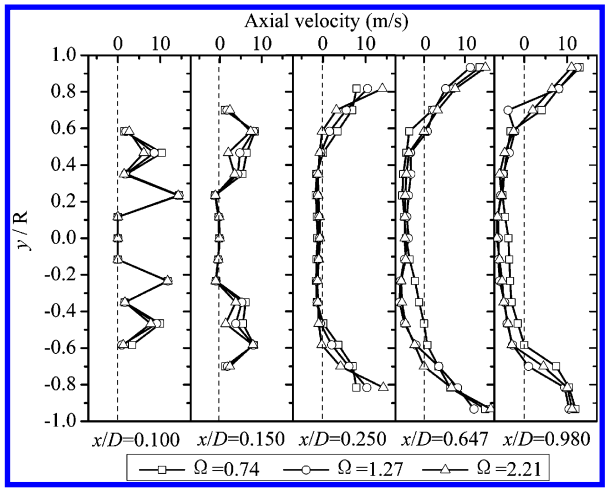

Figure 6. Profiles of the axial velocity at various inner SA swirling intensities.

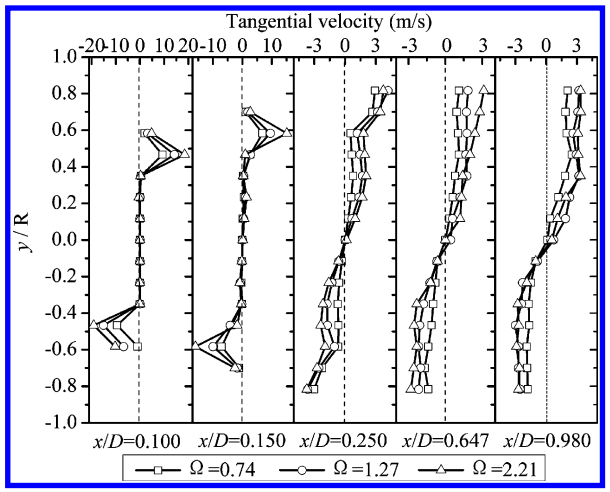

Figure 7. Profiles of the tangential velocity at various inner SA swirling intensities.

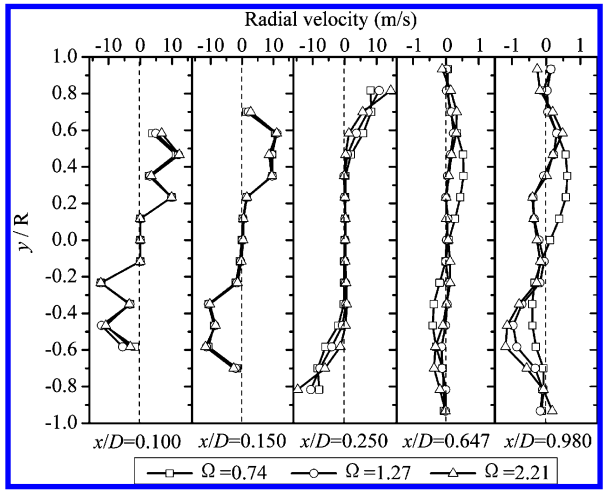

Figure 8. Profiles of the radial velocity at various inner SA swirling intensities.

indicated by the absence of the inner peak in the corresponding slices in Figure 6. At the same time, the jet of the outer SA has since become the dominant stream. As mentioned above, such great axial velocity near the wall of the burner provides a means

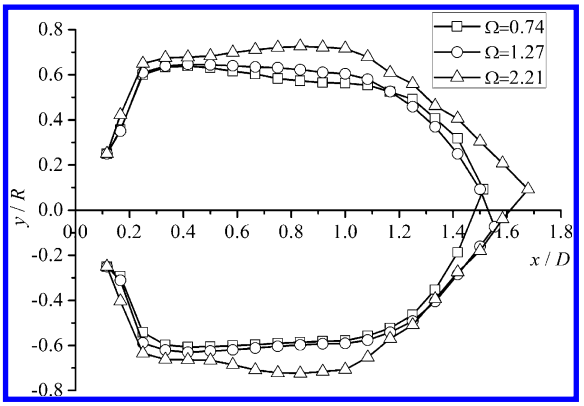

Figure 9. Recirculation zone boundary of the burner at various inner SA swirling intensities.

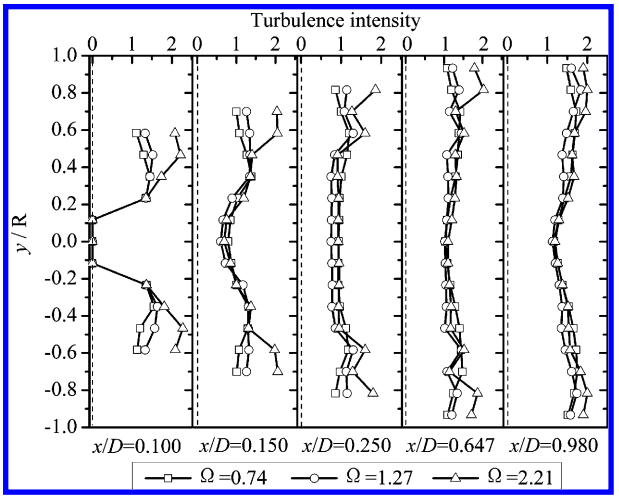

Figure 10. Profiles of turbulence intensity at various inner SA swirling intensities.

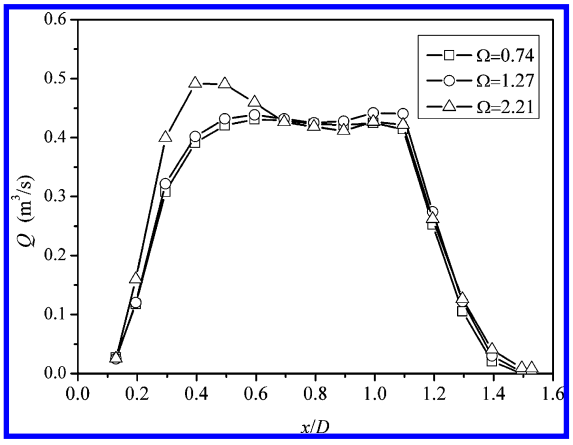

Figure 11. Variations of volumetric reflux at different inner SA swirling intensities.

to avoid slagging in the ACC and near the exit of the burner as well. The negative values of the axial velocity between x/D = 0.250 and 0.980 indicate the presence of a backflow zone. During operation of the burner, this backflow effect enables a continuous feeding of the HTFG to the vicinity of the PA nozzle, which improves both ignition of PC and flame stability.[16] In addition, the swirling intensity of the inner SA is shown to have negligible influence on the axial velocity in the

dx.doi.org/10.1021/ef301043x | Energy Fuels 2012, 26, 6640−6650

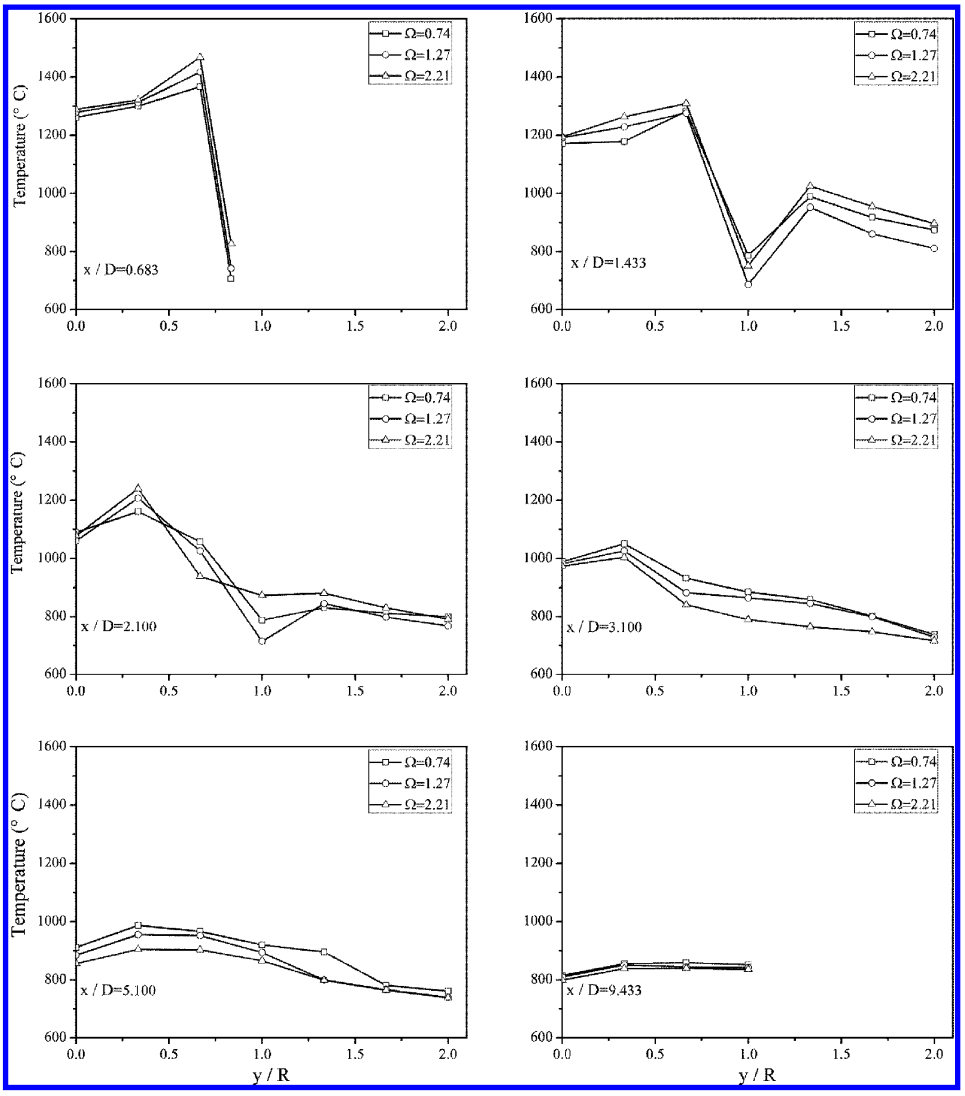

Figure 12. Temperature variations along the y direction at different cross sections of the ACC and furnace.

middle region of the burner, which is contrary to that observed by Chen et al.[17] due to the fact that in their experiment the mixing of the PA and SA took place in an unconfined region.

Near the exit of the PA and SA nozzles, the tangential velocity component vanishes in the vicinity of the bluff body, whereas it possesses a great value near the wall of the burner, as shown by the peaks in the slices corresponding to x/D = 0.100 and 0.150 in Figure 7. As expected, the tangential velocity component is increased as the swirling intensity of the inner SA becomes stronger. The tangential velocity decays rapidly along the axial direction due to the strong turbulence mixing effects, as shown by the slices for $x/D \geq 0.250$ in Figure 7 where the tangential velocity is low (<3 m/s). The observations in Figure 7 are in good agreement with the experimental results presented in the literature.[9,18]

A double-peak pattern is seen on the curves of the radial velocity component in the slices near the exit of the PA and SA nozzles (x/D < 0.250), as shown in Figure 8. The maximum value of the outer peak becomes higher with increasing swirling intensity of the inner SA. At x/D = 0.250, the maximum value of the radial velocity is found near the wall of the burner due to the jet of the outer SA. With further flow developing along the axial direction, the radial velocity drops gradually due to decay of the PA stream.

Comparison of the measured ICRZ boundaries for the three inner SA swirling intensities is presented in Figure 9. Formation of the bullet-shaped ICRZ is attributed to the combination effects of both the swirling inner SA and the bluff body. As the swirling intensity increases, both the diameter and length of the ICZR increase gradually. Similar to the arrangement in the previous figures, the profiles of the turbulence intensity at various axial locations are presented in Figure 10. The turbulence intensity T may be defined as

$$T = \sqrt{\overline{u'^2} + \overline{v'^2} + \overline{w'^2}}/\overline{u} \quad (5)$$

where $\overline{u'}$, $\overline{v'}$, and $\overline{w'}$ are the axial, tangential, and radial velocity fluctuations (m/s), respectively, and $\overline{u}$ is the mean velocity (m/s) of the burner jet.

In general, strong turbulence intensity is found at the boundary of the ICRZ, and becomes weak within it. The curve of T exhibits a single peak in the slices at x/D = 0.100 and 0.150 because of strong mixing between the PA and inner SA near the outlet of the burner nozzle. The turbulence intensity is enhanced with increasing swirling intensity of the outer SA for these two locations. Two peaks are seen in the slice at x/D =

dx.doi.org/10.1021/ef301043x | Energy Fuels 2012, 26, 6640−6650

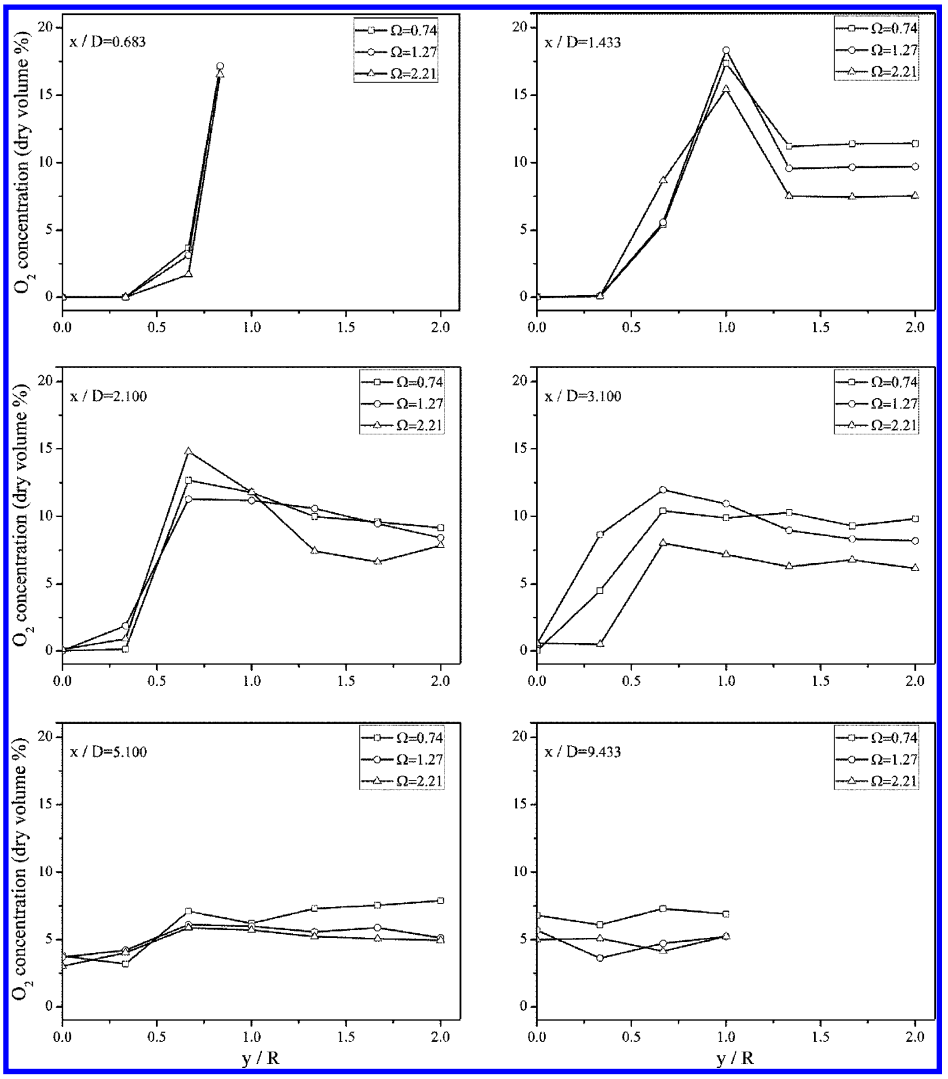

Figure 13. Variations of the O_2 concentration along the y direction at different cross sections of the ACC and furnace.

0.250 in Figure 10, with the inner one resulting from the shear velocity gradient at the boundary of the ICRZ and the outer one resulting from the introduction of the outer SA. The outer peak disappears for $x/D > 0.250$ as the outer SA mixes gradually with the main stream. Regions with large turbulence intensities are where PC burns intensively. Therefore, in practical operations, the ignition and combustion of PC are desired to be confined in these regions.[7]

The volumetric reflux Q (m^3/s) over a cross-sectional slice of the ICRZ, based on the recirculation velocity and the local radius r of the ICRZ, may be defined as

$$Q = 2\pi \int_0^R ur \, dr \tag{6}$$

where u is the back-flow velocity (m/s).

Variations of the volumetric reflux along the axial direction are presented in Figure 11 for the three swirling intensities of the inner SA. The curves are bell-shaped with a nearly flat top from $x/D = 0.4$ to 1.1 corresponding to the middle region of the ICRZ. It is clear that this peak is much wider than that observed by Zeng et al.[19] This extension of the region with strong recirculation is attributed to the presence of the bluff body. The left boundary ($x/D = 0.4$) of this region is due to the negative-pressure zone near the bluff body where the HTFG in the ACC is introduced backward. This region of high reflux was resulted from the relatively larger area of the backflow, as can be seen from Figure 9. The volumetric reflux increases slightly with raising swirling intensity of the inner SA. It is noted that, at the strongest swirling intensity observed ($\Omega = 2.21$), a significant increase at $x/D = 0.4$ is found with the maximum value being 0.49 m^3/s. Excessive volumetric reflux, however, might destroy the PA and inner SA nozzles. Therefore, a suitable swirling intensity of the inner SA should be utilized to reach a compromise between stable combustion and safe operation.[20,21]

4.2. Temperature Distributions and Gas Concentration. The experimental results from the combustion tests are presented as follows. The temperature variations along y direction at various axial locations, as labeled in Figure 5, in the ACC and furnace are presented in Figure 12, where the y values are scaled by the radius R of the ACC, $R = D/2$. In general, a greater swirling intensity of the inner SA leads to higher temperatures near the outlet of the burner and lower temperatures near the exit of the furnace. At $x/D = 0.683$ (in the ACC), the temperatures rise gradually and reach the peak values (around 1400 °C) at the boundary of the ICRZ ($y/R = 0.6$). While approaching the wall of the ACC, due to the presence of the outer SA, a sudden drop to low temperatures

dx.doi.org/10.1021/ef301043x | Energy Fuels 2012, 26, 6640−6650

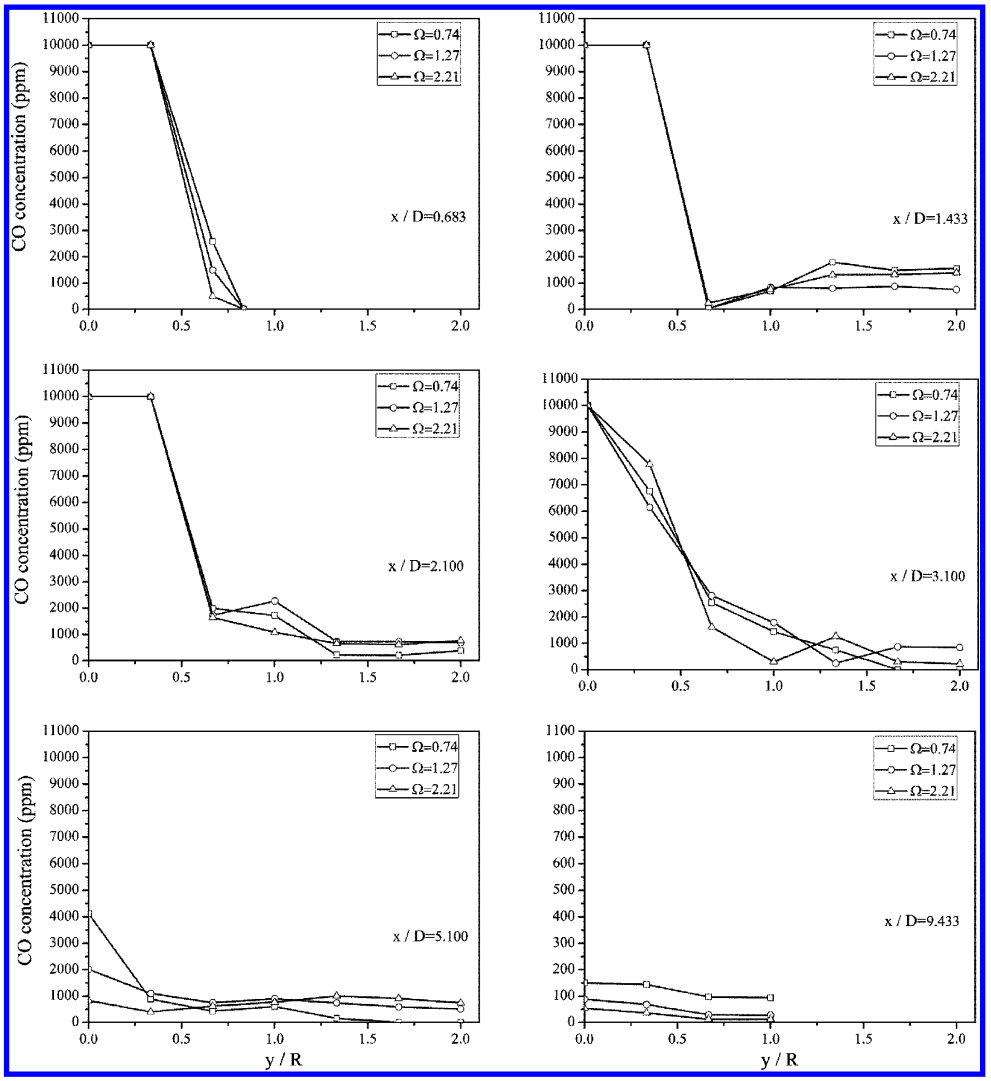

Figure 14. Variations of the CO concentration measured along the y direction at different cross sections of the ACC and furnace.

(around 800 °C) is found. This low level of temperature at the wall of ACC is desirable for preventing slagging. When entering the furnace ($x/D \geq 1.433$), the temperature curves for $y/R > 1.0$ feature an increase due to exothermic reactions of PC with the outer SA, followed by a slow drop toward the water-cooled wall. As expected, the temperature profiles are gradually flatten out, and the maximum values decrease along the axial direction. At the outlet of the furnace, the temperatures of the flue gas are rather uniform as a result of complete combustion of PC.[22]

The measured gas concentrations, including O_2, CO, and NO_x, are presented in the following figures. The O_2 concentration (dry volume percentage) profiles at various axial locations are shown in Figure 13. At $x/D = 0.683$ (in the ACC), the O_2 concentrations nearly vanish for $y/R < 0.3$ due to the recirculation of the HTFG, followed by an sharp increase to around 17% due to the introduction of the outer SA. When $x/D = 1.433$, the local drop of the O_2 concentrations at $y/R > 1.0$ is due to the consumption of oxygen in the outer SA, confirmed by the local temperature rise at the same location, as shown in Figure 12. It is noted that, near the water-cooled wall ($y/R > 1.3$), the O_2 concentration decreases as the swirling intensity of the inner SA becomes higher. When $x/D \geq 1.433$, the curves are gradually flatten out along the axial direction. The O_2 concentrations are found to be nearly 5% at the exit of the furnace, which indicates an excessive air ratio of approximately 1.3. In addition, O_2 concentrations remain at above 5% near the water-cooled wall for all the cases, which is desirable to avoid high temperature corrosion in these areas.

Figure 14 depicts the profiles of CO concentration at the various axial locations. When PC begins to burn, a large amount of O_2 is consumed during a short time period so that CO concentrations in the first slice increase sharply to exceed 10000 ppm, which was upper limit of MGA 5 gas analyzer. The CO concentrations decrease along the y direction due to the increase of O_2, as shown previously in Figure 13. At $x/D = 0.683$, it is shown that a greater swirling intensity of the inner SA leads to higher CO and lower O_2 concentration (see Figure 13) as a result of the occurrence of a high-temperature zone near the PA nozzle, which is beneficial to ignition and combustion of PC. The CO concentrations decrease along both x and y directions and finally become negligible at the exit of the furnace. It is noted that the CO concentration at the exit decreases with increasing swirling intensity.

Previous work has shown that the swirling intensity has an important effect on the NO_x emission for swirling PC combustors.[23−28] The profiles of the NO_x concentration (at 6% O_2) measured along the various axial locations are presented in Figure 15. At $x/D = 0.683$, the NO_x concentration

dx.doi.org/10.1021/ef301043x | Energy Fuels 2012, 26, 6640−6650

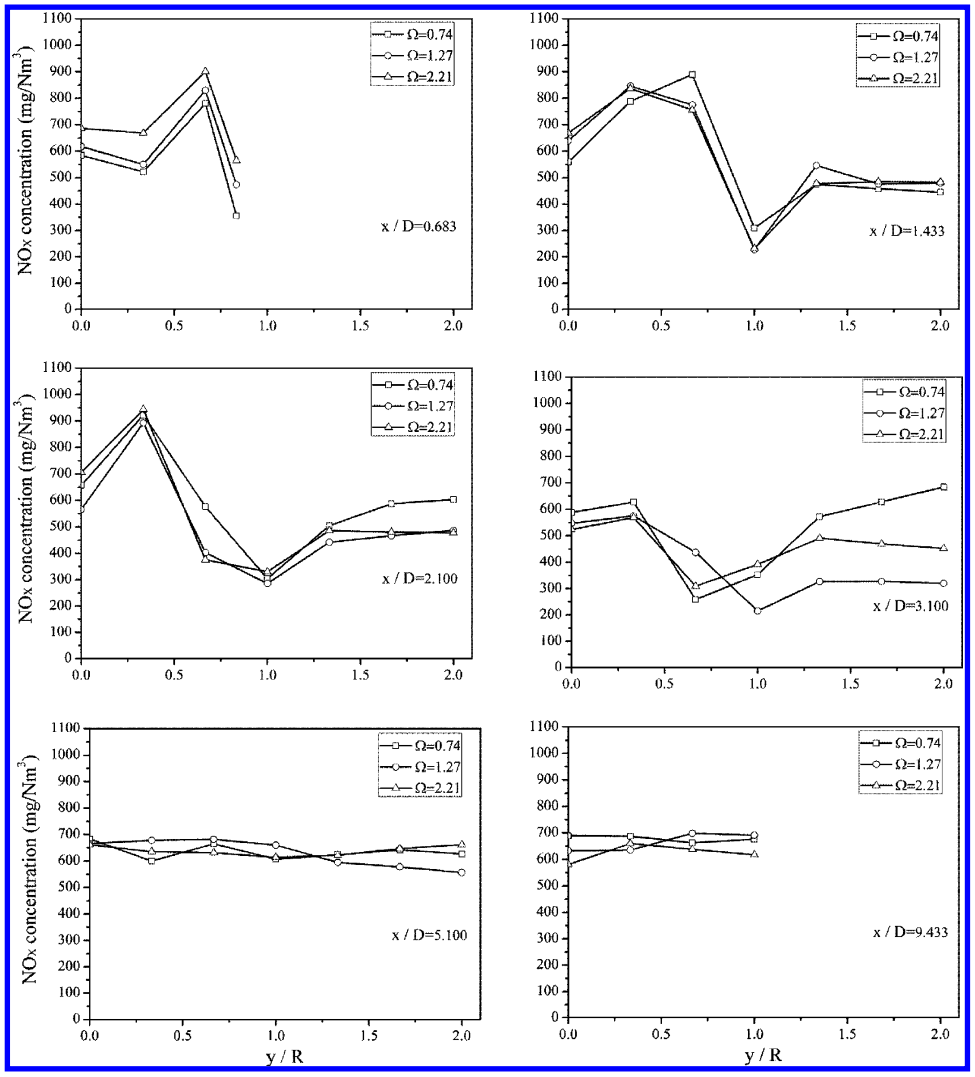

Figure 15. Variations of the NO_x concentration (at 6% O_2) measured along the y direction at different cross sections of the ACC and furnace.

Table 4. Variations of Unburned Carbon in Fly Ash and Boiler Operating Efficiency for Ω = 0.74, 1.27, and 2.21

no. of swirl intensity	unburned carbon in fly ash (%)	boiler operating efficiency (%)
0.74	10.56	89.65
1.27	8.87	90.35
2.21	7.53	91.08

increases with increasing swirling intensity. It is noted that the maximum NO_x concentration (around 800 mg/Nm^3) is found at the boundary (y/R = ~0.7 for $x/D \leq 1.433$) of the ICRZ observed in the cold air test (see Figure 9). The local condition at this boundary is expected to be stoichiometric, and a reduced NO_x emission can be induced. However, the unexpected local increase in NO_x concentration is because the ICRZ in combustion test was shrunk from the size observed in the cold air test, indicating that the local maximum NO_x concentration is actually found in the outer SA region where the slight fuel-lean condition was present.

Near the wall of the ACC, the NO_x concentration is even below 600 mg/Nm^3, which indicates that a low temperature (see Figure 12) tends to suppress NO_x formation. At x/D = 1.433, the local troughs around y/R = 1.0 are due to PC combustion in an environment of insufficient oxygen and high CO, as shown previously in Figures 13 and 14, respectively. While approaching the water-cooled wall, the NO_x formation increases slightly because of the existence of an oxidization environment. This is in a good agreement with the experimental observation by Li et al.[29] Due to the dilution effect, the curves gradually flatten out and the NO_x concentration at the exit of the furnace ranges between 550 and 700 mg/Nm^3, which is lower than the experimental data (844 mg/Nm^3) reported by Zeng et al.[10]

As mentioned, lowering the flue gas temperature has been realized as an effective approach to suppression of NO_x formation. This approach, however, is undesirable for stable combustion. The introduction of an outer SA without swirling, as proposed in the present study, enables the air-staged combustion effect[30−32] with 20% of the combustion air being injected by the outer SA, providing a promising means by which NO_x reduction, stable combustion, and slagging prevention can be achieved simultaneously.

Finally, to examine the degree of PC burnout, which is an important operation parameter of full-scale PC combustion, the unburned carbon in fly ash was measured, as listed Table 4. The boiler operating efficiency is also compared in Table 4 for the three swirling intensities of the inner SA. With increasing swirling intensity, the unburned carbon in fly ash is lowered,

dx.doi.org/10.1021/ef301043x | Energy Fuels 2012, 26, 6640−6650

while the boiler operating efficiency is increased. It is noted that the boiler operating efficiency is greater than 89.50% for all the swirling intensities studied.

5. CONCLUSIONS

A novel design of pulverized coal burner for industrial boilers, featuring the introduction of an outer secondary air without swirling, has been proposed in the present study. Both cold air and combustion tests of this novel pulverized coal burner have been performed. The measured flow fields, temperature distributions, and gas concentrations at three different swirling intensities of the inner secondary air have been presented and discussed. Conclusions can be drawn as follows:

(1) The formation of internal center recirculation zone was clearly observed due to the presence of the bluff body and swirling inner secondary air. A suitable swirling intensity of the inner secondary air should be chosen to reach a compromise between stable combustion and safe operation.

(2) The great axial velocity near the wall of the burner, due to the presence of the outer secondary air, can prevent slagging in the adiabatic combustion chamber.

(3) The air-staged combustion effect, enabled by the presence of the outer secondary air without swirling, can suppress NO_x emission of the industrial boiler to around 600 mg/Nm^3.

(4) The boiler operating efficiency was higher than that of the conventional industrial boilers, which was found to be greater than 89.50% for all the swirling intensities tested.

(5) Due to the outer secondary air, combustion proceeds outside the internal center recirculation zone, which results in local high temperature and NO_x generation. In an effort to completely evaluate the performance of the burners with this novel design, a more in-depth investigation of NO_x emissions and a comparison with the use of swirling outer secondary air are required in future studies.

AUTHOR INFORMATION

Corresponding Author

*Tel./fax: 86-029-82665185. E-mail: dfche@mail.xjtu.edu.cn.

Notes

The authors declare no competing financial interest.

ACKNOWLEDGMENTS

The financial support provided by Zhejiang Provincial Science and Technology Major Project through Grant No. 2008C13013 is gratefully acknowledged.

NOMENCLATURE

D = diameter of the adiabatic combustion chamber, m
K = axial momentum, kg m/s^2
L = characteristic length, m
M = rotary momentum moment, kg m^2/s^2
q = volumetric flow rate, m^3/s
Q = volumetric reflux, m^3/s
r = local radius, m
R = radius of the adiabatic combustion chamber, m
T = turbulence intensity
u = back-flow velocity, m/s
$\overline{u}$ = mean velocity of the burner jet, m/s
$\overline{u'}$ = axial velocity fluctuation, m/s
$\overline{v'}$ = tangential velocity fluctuation, m/s
$\overline{w'}$ = radial velocity fluctuation, m/s

Greek Symbols

ρ = density, kg/m^3
ω = velocity component, m/s
Ω = swirling intensity

Subscripts

a = axial
t = tangential

REFERENCES

(1) Fang, J. H.; Zeng, T. F.; Lynn, I.; Yang, S.; Oye, K. A.; Sarofim, A. F.; Beer, J. M. Coal utilization in industrial boilers in China—a prospect for mitigating CO_2 emissions. *Appl. Energy* **1999**, *63*, 35−52.

(2) Wang, F. Y.; Yang, J. C.; Zhang, R. Z.; Xu, Z. Q. Medium-and small-boilers change to CWM burning: Some technical problems. *China Coal* **2003**, *9*, 45−46 (in Chinese)..

(3) Xie, Y. G.; Zhang, C. M.; Wang, F. Y.; Zhao, X. The combustion test and analysis of a 2.8 MW hot-water traveling-grate boiler retrofitted for firing coal-water slurry. *J. Eng. Therm. Energy Power* **1999**, *19*, 309−311 (in Chinese)..

(4) Feng, J. K. Experience of industrial boilers burning pulverized coal. *Boiler Technol.* **1989**, *11*, 9−11 (in Chinese)..

(5) Pang, L. J.; Chen, G. F.; Chen, C. S.; Qin, Y. K.; Xie, Y. L.; Hu, R. D. A new PW-1 type of pulverized coal burner. *Energy Conserv. Technol.* **1994**, *3*, 9−12 (in Chinese).

(6) Ji, R. S. Numerical simulation of combustion in the industrial pulverized-coal boiler. *J. China Coal Soc.* **2009**, *34*, 1703−1706 (in Chinese).

(7) You, C. F.; Zhou, Y. Effect of operation parameters on the slagging near swirl near swirl coal burner throat. *Energy Fuels* **2006**, *20*, 1855−1861.

(8) Zeng, L. Y.; Li, Z. Q.; Cui, H.; Zhang, F. C.; Chen, Z. C.; Zhao, G. B. Effect of fuel bias distribution in the primary air nozzle on the slagging near a swirl coal burner throat. *Energy Fuels* **2009**, *23*, 4893−4899.

(9) Jing, J. P.; Li, Z. Q.; Liu, G. K.; Chen, Z. C.; Ren, F. Influence of different outer secondary air vane angles on flow and combustion characteristics and NO_x emissions of a new swirl coal burner. *Energy Fuels* **2010**, *24*, 346−354.

(10) Zeng, L. Y.; Li, Z. Q.; Zhao, G. B.; Shen, S. P.; Zhang, F. C. Numerical simulation of combustion characteristics and NO_x emissions in a 300 MWe utility boiler with different outer secondary-air vane angles. *Energy Fuels* **2010**, *24*, 5349−5358.

(11) Jing, J. P.; Li, Z. Q.; Zhu, Q. Y.; Chen, Z. C.; Wang, L.; Chen, L. Z. Influence of the outer secondary air vane angle on the gas/particle flow characteristics near the double swirl flow burner region. *Energy* **2011**, *36*, 258−267.

(12) Jing, J. P.; Li, Z. Q.; Wang, L.; Chen, L. Z.; Yang, G. H. Influence of secondary air mass flow rates on gas/particle flow characteristics near the swirl burner region. *Energy* **2011**, *36*, 3599−3605.

(13) Jing, J. P.; Li, Z. Q.; Wang, L.; Chen, Z. C.; Chen, L. Z.; Zhang, F. C. Influence of the mass flow rate of secondary air on the gas/particle flow characteristics in the near-burner region of a double swirl flow burner. *Chem. Eng. Sci.* **2011**, *66*, 2864−2871.

(14) Zeng, L. Y.; Li, Z. Q.; Zhao, G. B.; Shen, S. P.; Zhang, F. C. Effect of the vane angle for outer secondary air on the flow and combustion characteristics and NO_x emissions of the low-NO_x axial-swirl coal burner. *Numer. Heat Transfer, Part A* **2011**, *59*, 43−57.

(15) Chi, Z.; Ding, S.; Cheng, D.; Wang, J.; Deng, L.; Sun, G.; Liu, F.; Guan J.; Wang, J.; Zeng, X.; Zhu, L. Chinese Patent No. 200910101889.1, Feburary 2, 2011.

(16) Zhang, H.; Yue, G.; Lu, J.; Jia, Z.; Mao, J.; Fujimori, T.; Suko, T.; Kiga, T. Development of high temperature air combustion technology

in pulverized fossil fuel fired boilers. *Proc. Combust. Inst.* **2007**, *31*, 2779−2785.
(17) Chen, Z; Li, Z; Jing, J; Chen, L; Wu, S; Yao, Y. Gas/particle flow characteristics of two swirl burners. *Energy Conserv. Manage.* **2009**, *50*, 1180−1191.
(18) Tsioumanis, N.; Brammer, J.; Hubert, J. Flow processes in a radiant tube burner: Isothermal flow. *Fuel* **2008**, *87*, 103−111.
(19) Zeng, L.; Li, Z; Zhao, G; Li, J; Zhang, F; Shen, S; Chen, L. The influence of swirl burner structure on the gas/particle flow characteristics. *Energy* **2011**, *36*, 6184−6194.
(20) Zhao, L.; Zhou, Q.; Zhao, C. Flame characteristics in a novel petal swirl burner. *Combust. Flame* **2008**, *155*, 277−288.
(21) Stone, C.; Menon, S. Swirl control of combustion instabilities in a gas turbine combustor. *Proc. Combust. Inst.* **2002**, *29*, 155−160.
(22) Kaewklum, R.; Kuprianov, V. Experimental studies on a novel swirling fluidized-bed combustor using an annular spiral air distributor. *Fuel* **2010**, *89*, 43−52.
(23) Godoy, S.; Hirji, K. A.; Lockwood, F. C. Combustion measurements in a pulverized coal-fired furnace. *Combust. Sci. Technol.* **1988**, *59*, 165−182.
(24) Abbas, T.; Costen, P.; Hassan, M. A.; Lockwood, F. C. The effect of the near burner aerodynamics on pollution, stability, and combustion in a PF-fired furnace. *Combust. Sci. Technol.* **1993**, *93*, 73−90.
(25) Van der Lans, R. P.; Glarborg, P.; Dam-Johansen, K. Influence of process parameters on nitrogen oxide formation in pulverized coal burners. *Prog. Energy Combust. Sci.* **1997**, *23*, 349−377.
(26) Gu, M. Y.; Zhang, M. C.; Fan, W. D.; Wang, L.; Tian, F. D. The effect of the mixing characters of primary air and secondary air on NO_x formation in a swirling pulverized coal flame. *Fuel* **2005**, *84*, 2093−2101.
(27) Xue, S.; Hui, S. E.; Zhou, Q. L.; Xu, T. M. Experimental study on NO_x emission and unburnt carbon of a radial biased swirl burner for coal combustion. *Energy Fuels* **2009**, *23*, 3558−3564.
(28) Xue, S.; Hui, S. E.; Liu, T. S.; Zhou, Q. L.; Xu, T. M.; Hu, H. L. Experimental invetigation on NOx emission and carbon burnout from a radially biased pulverized coal whirl burner. *Fuel Process. Technol.* **2009**, *90*, 1142−1147.
(29) Li, Z; Jing, J; Liu, G; Chen, Z; Liu, C. Measurement of gas species, temperatures, char burnout, and wall heat fluxes in a 200-MWe lignite-fired boiler at different loads. *Appl. Energy* **2010**, *87*, 1217−1230.
(30) Ballester, J.; Sanz, A.; Gonzalez, M. A. Investigation of the characteristics and stability of air-staged flames. *Exp. Therm. Fluid Sci.* **2008**, *32*, 776−790.
(31) Zhang, Y.; Zhou, L.; Wei, X.; Sheng, H. Studies of effect of a coal concentrator on NO formation in swirling coal combustion. *Int. J. Heat Mass Transfer* **2006**, *49*, 421−426.
(32) Nettleton, M. A. The influence of swirl angles on flame stability in pilot-scale plant. *Fuel* **2004**, *83*, 253−256.